

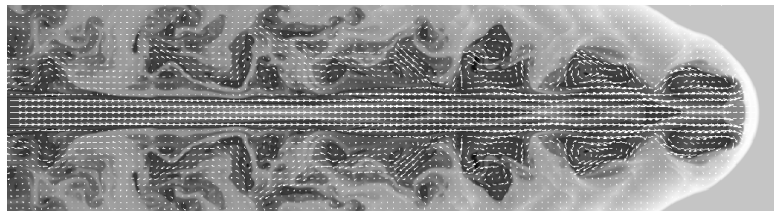
Magnetized relativistic jets: Exploring the internal structure with numerical simulations

José M^a Martí

Departamento de Astronomía y Astrofísica
Universidad de Valencia (Spain)



VNIVERSITAT DE VALÈNCIA



Blazars through Sharp Multiwavelength Eyes
Málaga, 30 May - 3 June 2016
Celebrating 30+ years of Alan Marscher's contributions to the physics of blazars...

Exploring the internal structure of RMHD jets with numerical simulations: Introduction

Quasi-steady VLBI components in AGN jets are interpreted as **recollimation shocks** (e.g. [Daly & Marscher 1988](#)) since the first fluid dynamical models of extragalactic radio sources.

Multi-wavelength observations associate **γ -ray flares** with the passing of new superluminal components through the mm-VLBI core (e.g., BL Lac, PKS 1510 - 089; [Marscher et al. 2008, 2010](#)) or distant standing components (e.g., HST-1 complex in M87; [Cheung et al. 2007, Giroletti et al. 2012](#)).

- The increase in particle and magnetic energy required to power the flares are explained by identifying the **mm-VLBI radio core/standing component** with a **recollimation shock**.

Dynamically important magnetic fields appear associated with the currently accepted jet formation mechanisms ([Blandford & Payne 1982; Li et al. 1992; Blandford & Znajek 1977](#))

- Studies of **Faraday-corrected polarization vector** in the inner-pc jet of BL Lac suggests that the jet is threaded by a **helical magnetic field** ([Gómez et al. 2016](#)).

Many other observations point towards a **complex transversal structure** in pc-scale jets (e.g., **top/down jet asymmetries** in total and polarized emission, 1055+018, [Attridge et al. 1999](#))

One of the approaches to test all these hypotheses is to characterize the internal structure (transversal structure, internal shocks, ...) of magnetized relativistic jets by means of numerical (RMHD) simulations

Transversal equilibrium of RMHD jets: The role of flow rotation and magnetic tension (I)

Model assumptions:

Cylindrical coordinates (r, ϕ, z) :

- Axisymmetry $\partial_\phi = 0$
- Planar symmetry along the jet axis $\partial_z = 0$
- Steady flow $\partial_t = 0$

Under these conditions, **6 functions** of the cylindrical radial coordinate are needed to characterize the flow:

$$\rho(r), \quad p(r), \quad v^\phi(r), \quad v^z(r), \quad B^\phi(r), \quad B^z(r)$$

(gas density and pressure; azimuthal and axial components of flow velocity and magnetic field)

$(v^r(r) = 0, \quad B^r(r) = 0$, because of the b.c. at the jet axis and the condition $\partial_z = 0$) and

the ambient pressure, p_a , characterizing the homogeneous unmagnetized ambient medium at rest.

Transversal equilibrium:

$$\boxed{\frac{dp}{dr} = f(r, \rho, p, v^\phi, v^z, B^\phi, B^z)}$$

to be solved for $p(r)$ with fixed profiles of the remaining variables (and proper b.c. at the jet surface).

Transversal equilibrium of RMHD jets: The role of flow rotation and magnetic tension (II)

$$p^* = p(\rho, \varepsilon) + \frac{b^2}{2} \quad (\text{total pressure: thermal + magnetic})$$

$$h^* = h(\rho, \varepsilon) + \frac{b^2}{\rho} \quad (\text{total specific enthalpy})$$

$h(\rho, \varepsilon)$: specific enthalpy

ε : specific internal energy

$$W = \frac{1}{\sqrt{1 - v^2}} \quad (\text{flow Lorentz factor})$$

$$(b^0, \vec{b}) = \left(W(\vec{v} \cdot \vec{B}), \frac{\vec{B}}{W} + W(\vec{v} \cdot \vec{B}) \vec{v} \right)$$

(magnetic field four-vector in the comoving frame)

Transversal equilibrium:

$$\frac{dp^*}{dr} = \frac{\rho h^* W^2 (v^\phi)^2}{r} - \frac{(b^\phi)^2}{r}$$

Centrifugal force term
(>0 ; tends to decrease p^* inwards)

Magnetic tension term
(<0 ; tends to increase p^* inwards)

Units: $R_j = 1$
 $c = 1$
 $\rho_a = 1$

Boundary conditions:

$$p^*(R_{j,-}) = p^*(R_{j,+}) \quad (= p_a)$$

Transversal equilibrium of RMHD jets: The role of flow rotation and magnetic tension (III)

Top-hat profiles for density, axial flow velocity and axial magnetic field:

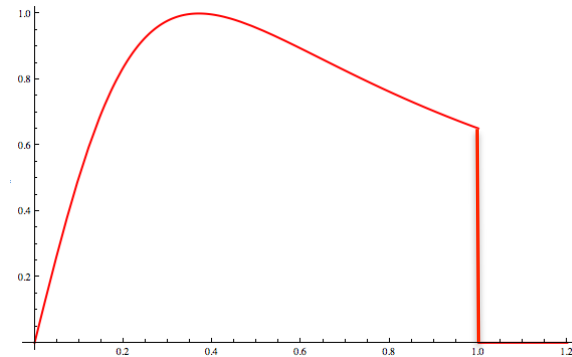
$$\rho(r) = \begin{cases} \rho_j, & 0 \leq r \leq 1 \\ 1, & r > 1, \end{cases}$$

$$v^z(r) = \begin{cases} v_j^z, & 0 \leq r \leq 1 \\ 0, & r > 1, \end{cases}$$

$$B^z(r) = \begin{cases} B_j^z, & 0 \leq r \leq 1 \\ 0, & r > 1, \end{cases}$$

Toroidal magnetic field:

$$B^\phi(r) = \begin{cases} \frac{2B_{j,m}^\phi(r/R_{B^\phi,m})}{1 + (r/R_{B^\phi,m})^2}, & 0 \leq r \leq 1 \\ 0, & r > 1. \end{cases}$$

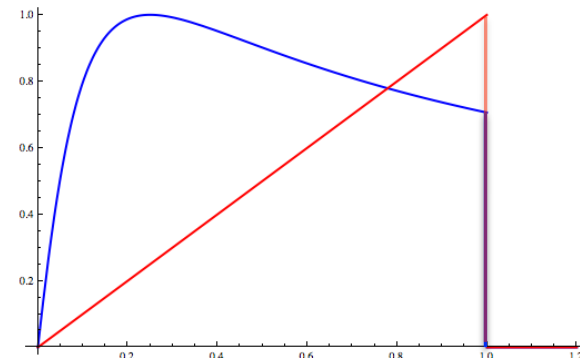


Three rotation laws:

No rotation: $v^\phi(r) = 0$.

Rigid rotation: $v^\phi(r) = \begin{cases} v_{j,m}^\phi r, & 0 \leq r \leq 1 \\ 0, & r > 1. \end{cases}$

Differential rotation: $v^\phi(r) = \begin{cases} \frac{3v_{j,m}^\phi(r/R_{v^\phi,m})}{1 + 2(r/R_{v^\phi,m})^{3/2}}, & 0 \leq r \leq 1 \\ 0, & r > 1. \end{cases}$



Transversal equilibrium of RMHD jets: The role of flow rotation and magnetic tension (IV)

$$\rho_j = 0.01$$

$$v_j^z = 0.97$$

$$B_j^z = 0.436 \text{ (left panel)}, 0.436 \times 10^{-2} \text{ (right panel)}$$

$$B_{j,m}^\phi = 1.58 \times 10^{-3} \text{ (left panel)}, 2.81 \text{ (right panel)}$$

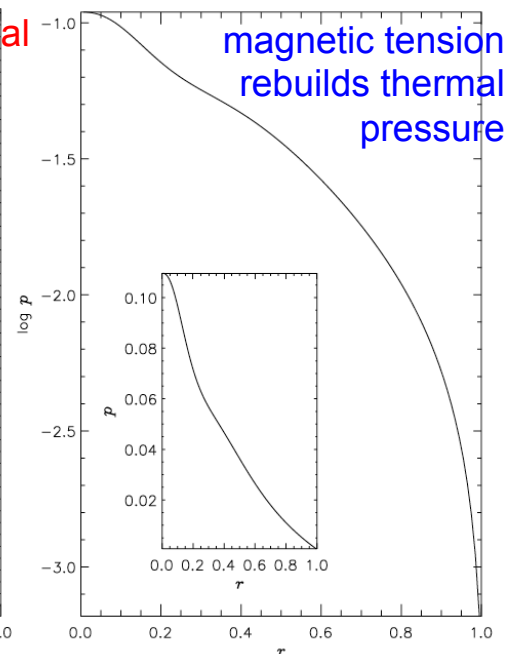
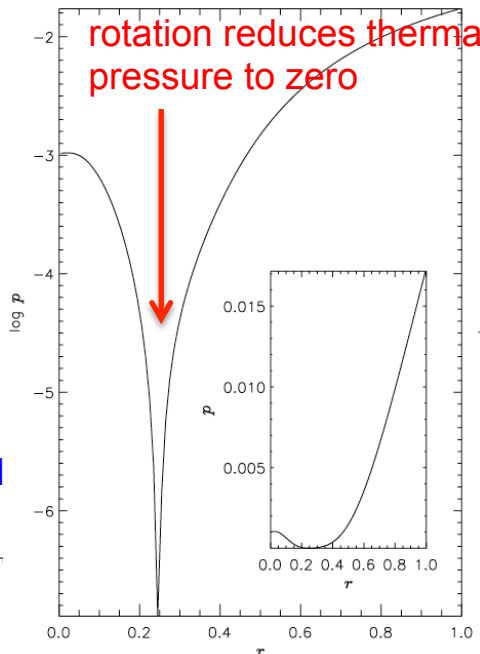
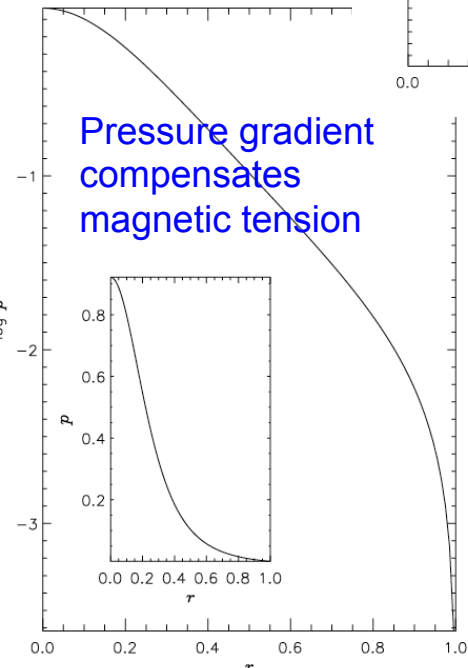
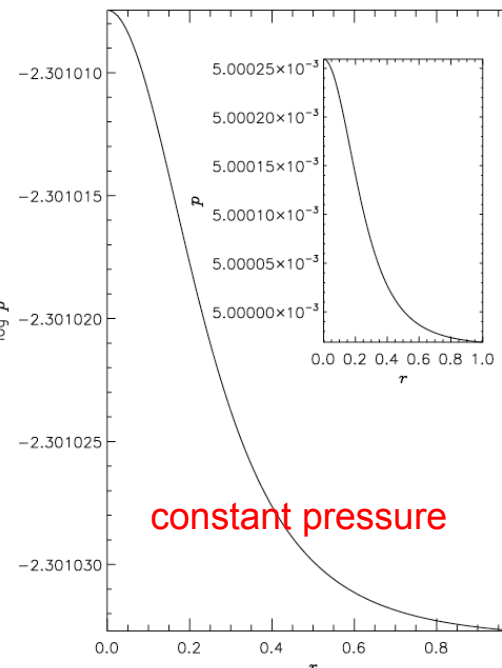
$$R_{B^\phi, m} = 0.37$$

$$p_a = 0.1$$

No rotation

weak toroidal magnetic field

stronger toroidal magnetic field



constant pressure

Pressure gradient compensates magnetic tension

weak toroidal magnetic field

stronger toroidal magnetic field

$$\rho_j = 0.01$$

$$v_j^z = 0.97$$

$$B_j^z = 0.396 \text{ (left panel)}, 0.441 \text{ (right panel)}$$

$$B_{j,m}^\phi = 0.151 \text{ (left panel)}, 0.443 \text{ (right panel)}$$

$$R_{B^\phi, m} = 0.37$$

$$v_{j,m}^\phi = 0.20$$

$$R_{v^\phi, m} = 0.25$$

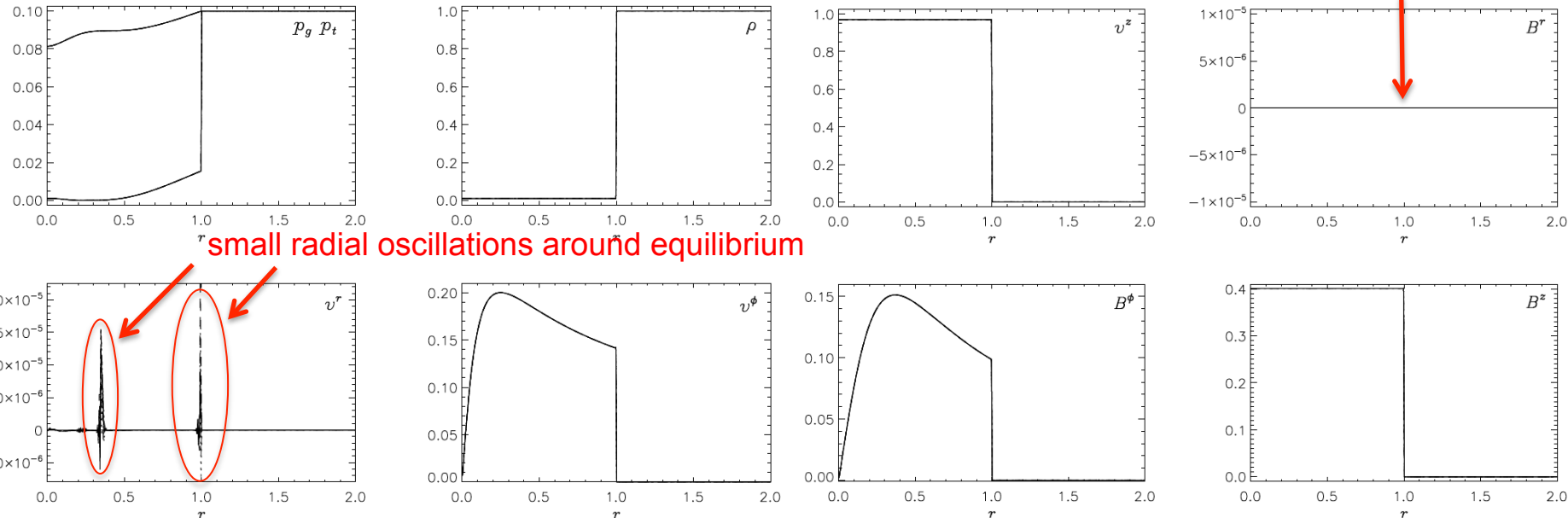
Differential rotation

$$p_a = 0.1$$

Transversal equilibrium of RMHD jets: 1D time-dependent simulations

Differential rotation, weak magnetic field case:

No spurious radial magnetic field generated



$t = 0, 100, 110, 120, 130, 140, 150$ (approx. 36 transversal light crossing times of the jet radius)

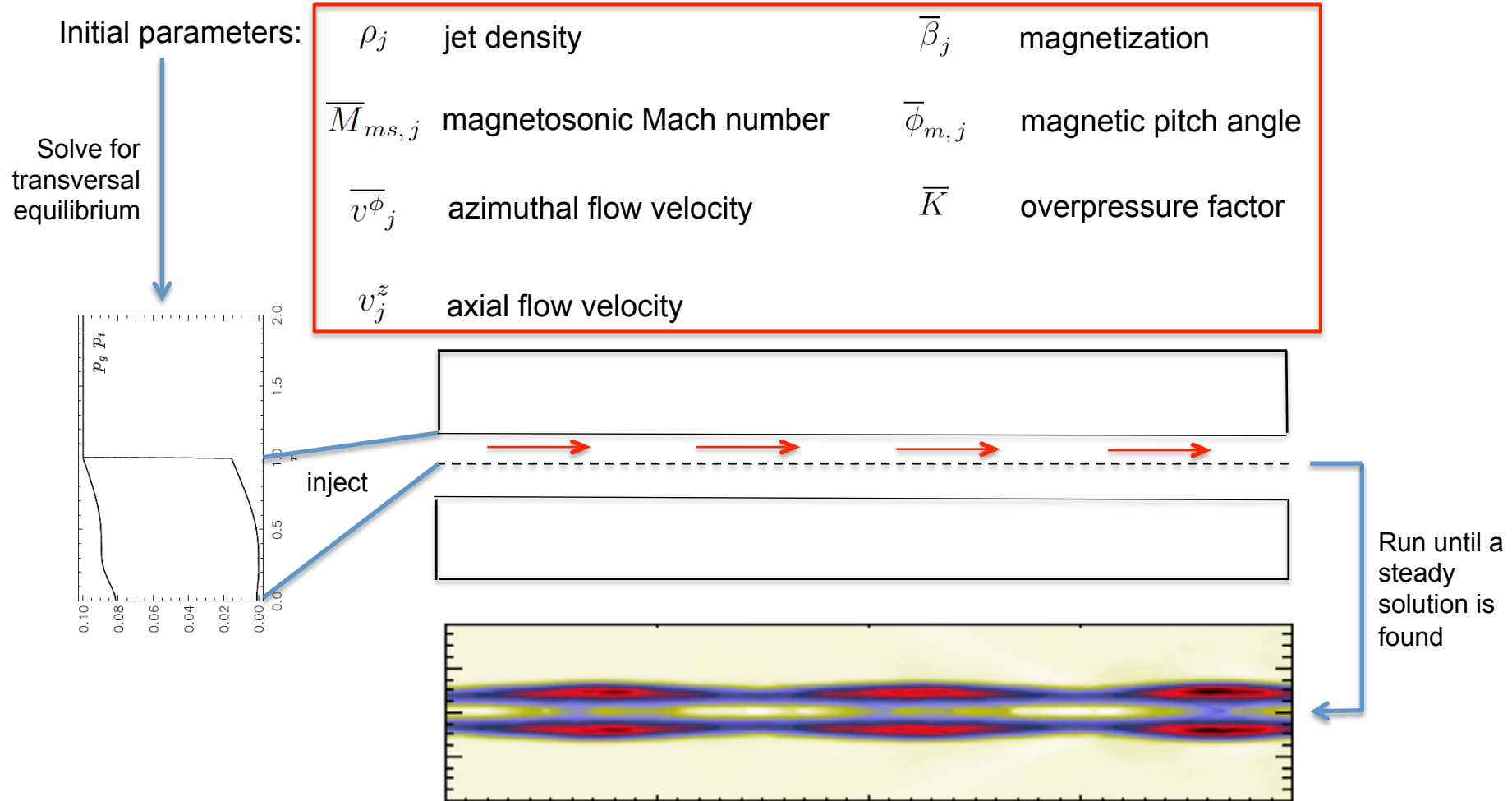
Mean relative errors inside the jet ($t = 150$; 200 cells/jet radius):

Model	p	ρ	v^ϕ	v^z	B^ϕ	B^z
DR	$< 10^{-3}$	$< 2 \times 10^{-4}$	$< 4 \times 10^{-6}$	$< 5 \times 10^{-7}$	$< 10^{-5}$	$< 10^{-5}$
RR	$< 3 \times 10^{-4}$	$< 2 \times 10^{-4}$	$< 10^{-4}$	$< 10^{-6}$	$< 5 \times 10^{-5}$	$< 2 \times 10^{-4}$

Conservative, second-order, finite-volume, constrained-transport code based on high-resolution shock-capturing methods (Martí 2015a, Martí 2015b)

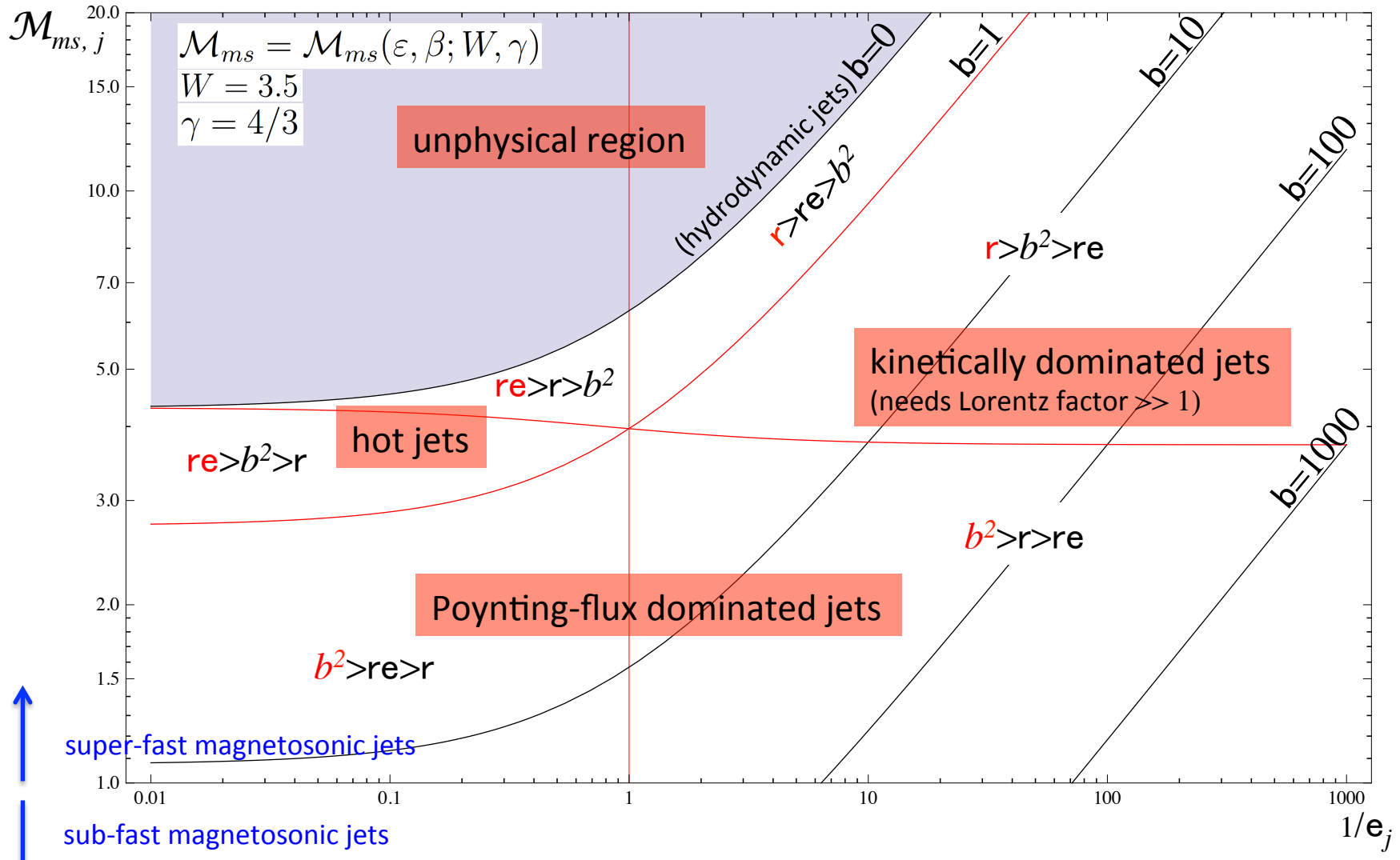
Internal structure of axisymmetric, overpressured RMHD jets (I): experiment setup

The plan is to inject these 1D solutions in transversal equilibrium into an axisymmetric cylindrical domain with a smaller ambient pressure, and wait until a 2D steady solution has settled.

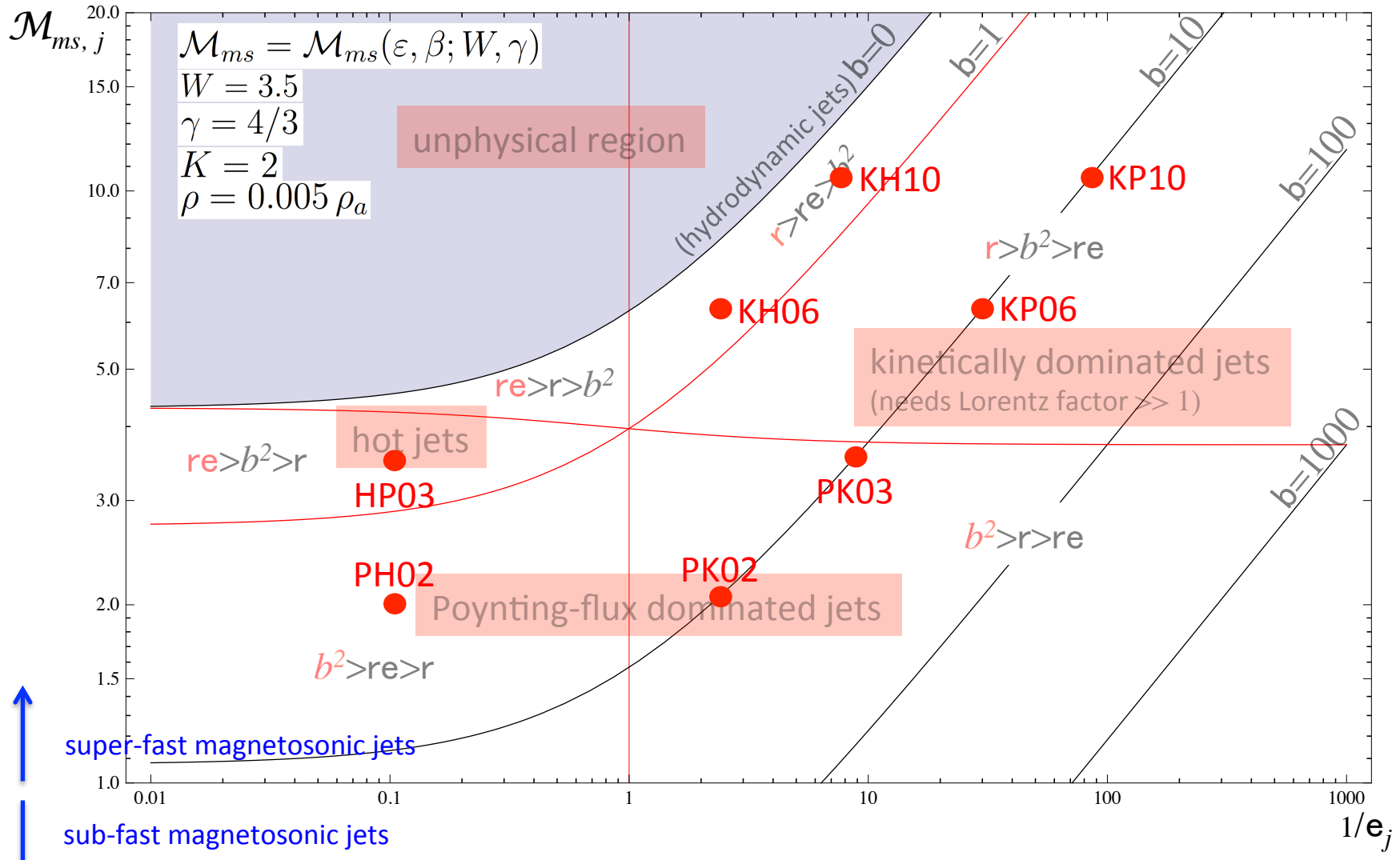


The aim is to minimize the sideways perturbations once immersed in the ambient medium to obtain an internal structure as clean as possible.

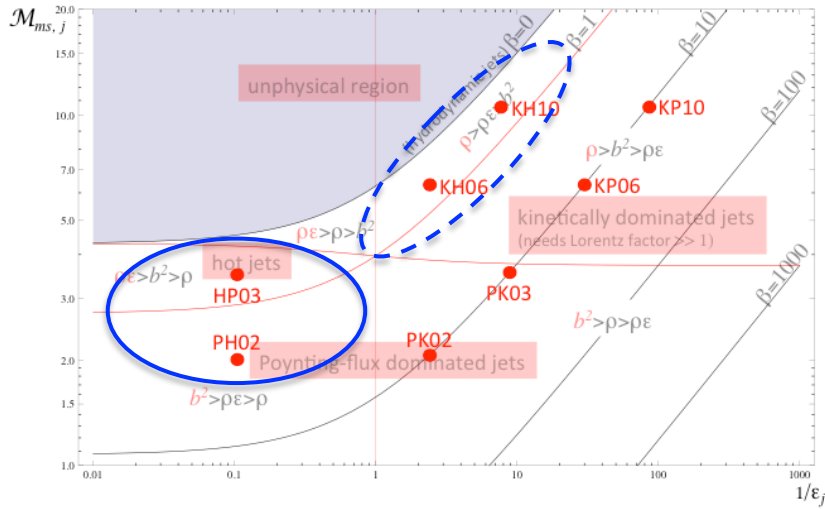
Internal structure of axisymmetric, overpressured RMHD jets (II):
Jet models in the Relativistic magnetosonic Mach number - specific internal energy diagram



Internal structure of axisymmetric, overpressured RMHD jets (II):
Jet models in the Relativistic magnetosonic Mach number - specific internal energy diagram

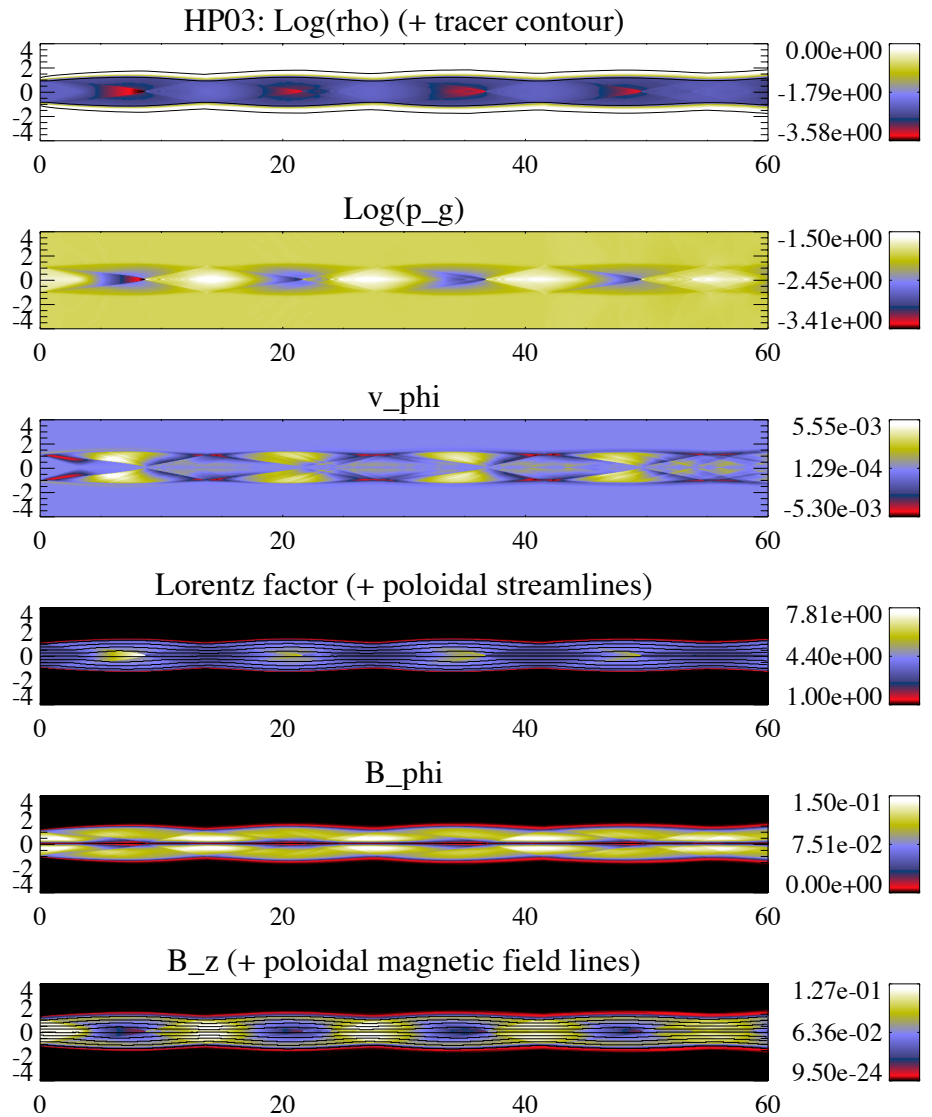


Internal structure of axisymmetric, overpressured RMHD jets: Results (I)

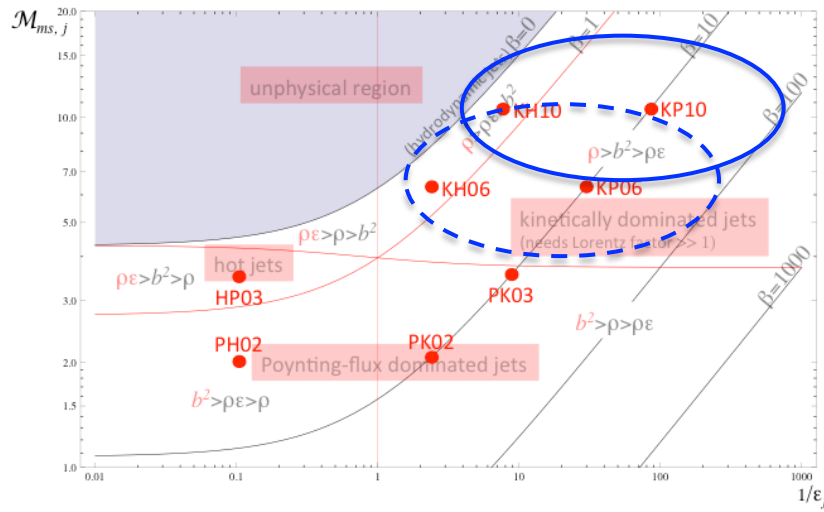


Hot jets (PH02, HP03):

- Rich internal structure characterized by conical (fast magnetosonic) shocks with short-wavelength axial periodicity
- Substantial internal energy to be converted into kinetic energy at jet expansions and back to internal energy at shocks
- Largest variations in flow Lorentz factor.

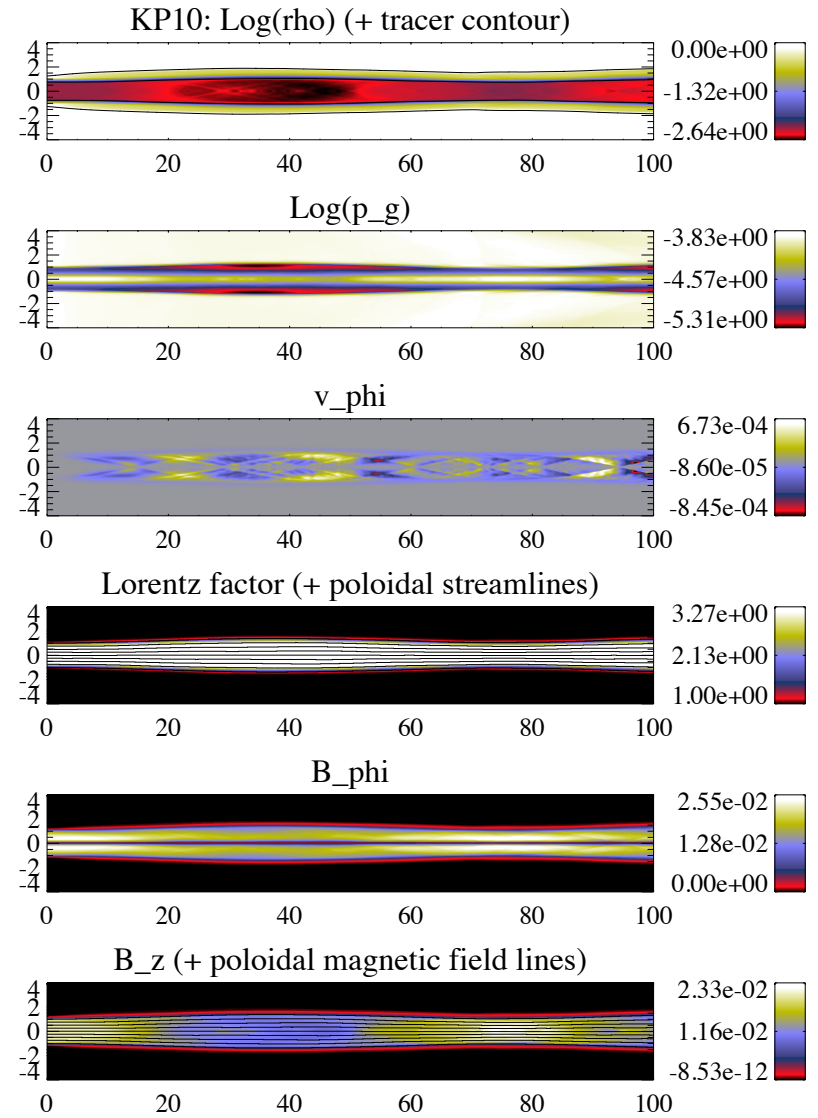


Internal structure of axisymmetric, overpressured RMHD jets: Results (II)

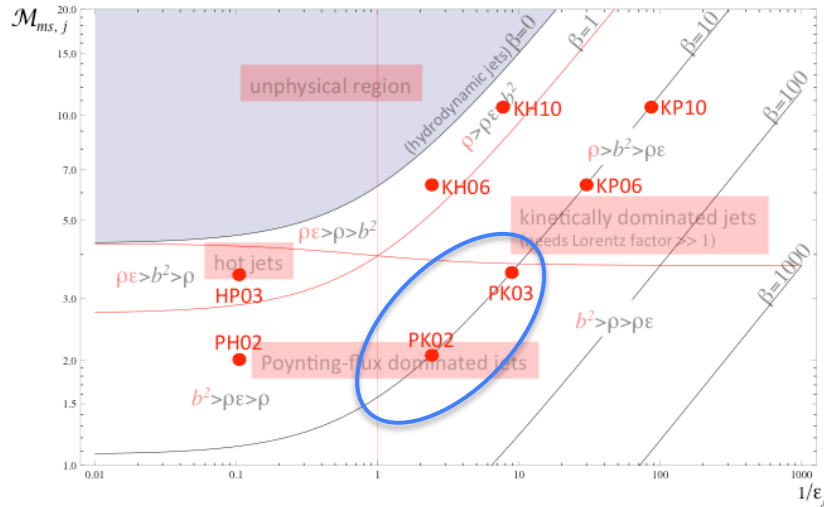


Kinetically dominated jets (KH10, KP10):

- Poor internal structure characterized by radial jet oscillations with long-wavelength axial periodicity
- No internal energy to exchange for kinetic energy
[Bernoulli mechanism does not operate]
- Almost constant flow Lorentz factor
- “Hot” central spine in high-magnetization jets, due to the magnetic tension of the toroidal field

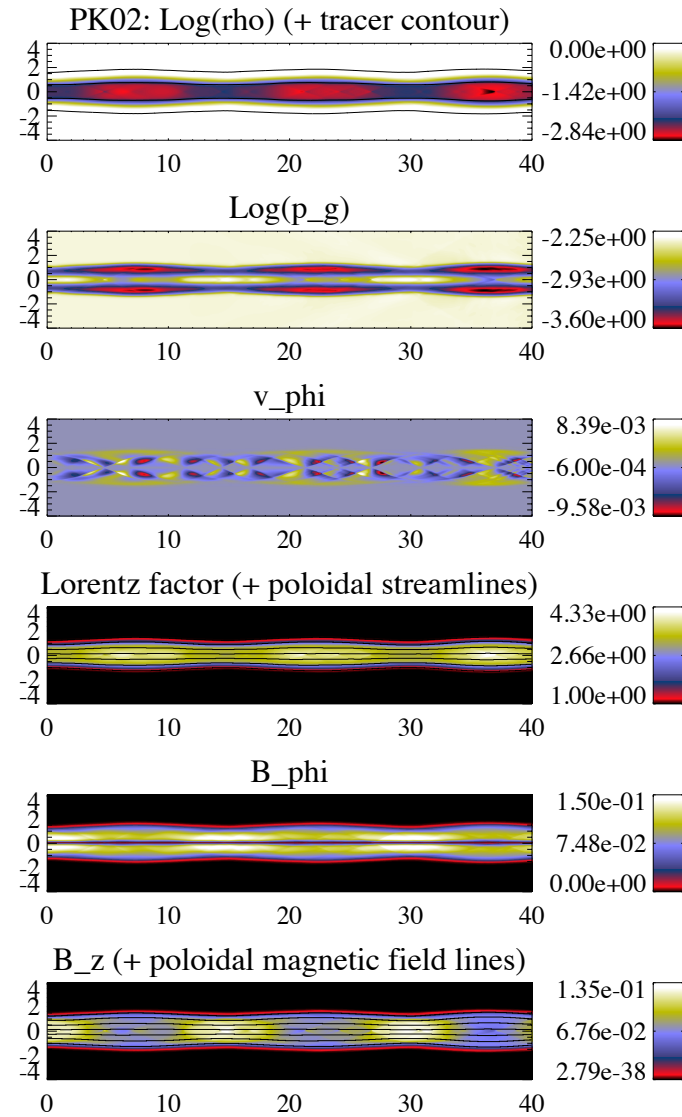


Internal structure of axisymmetric, overpressured RMHD jets: Results (III)

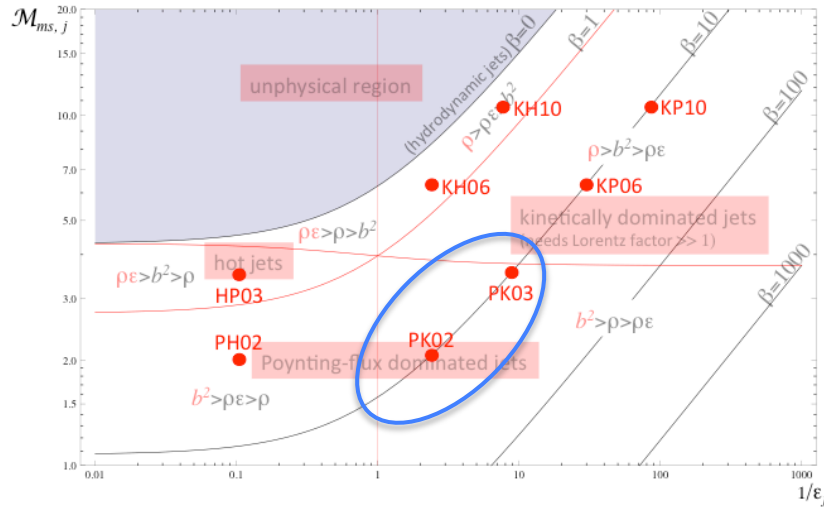


Poynting-flux dominated jets (PK02, PK03):

- Internal structure (shocks/jet oscillations, wavelengths,...) depends on the amount of internal energy
- “Hot” central spine depending on magnetization
- Prone to be unstable against magnetic pinch modes
[jets need wide shear layer to be stabilized and reach a steady solution] [the shear layer can change the internal structure of the jets]



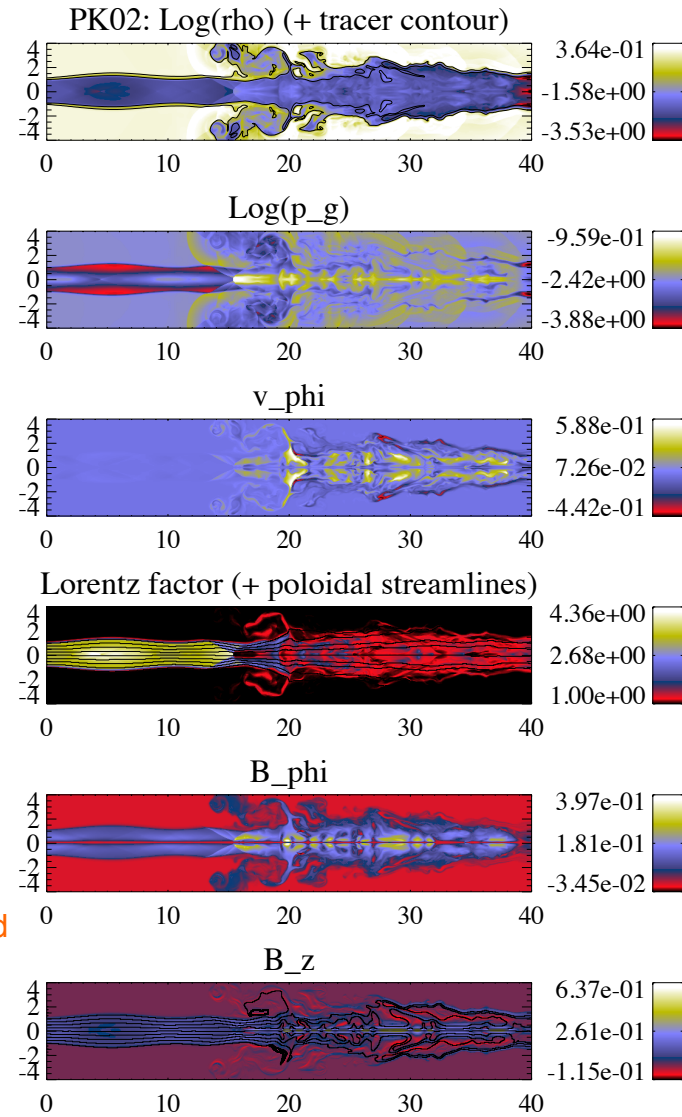
Internal structure of axisymmetric, overpressured RMHD jets: Results (III)



Poynting-flux dominated jets (PK02, PK03):

- Internal structure (shocks/jet oscillations, wavelengths,...) depends on the amount of internal energy
- “Hot” central spine depending on magnetization
- Prone to be unstable against magnetic pinch modes
[“Real” jets have small magnetizations (~ 1), unless stabilized by wide enough shear layers]

Same model, thinner shear layer



Internal structure of axisymmetric, overpressured RMHD jets: Results (IV)

Small (non-zero) azimuthal flow velocities generated in all the models as a result of the jet expansion

Lorentz force:

$$\vec{F}_L = \vec{J} \times \vec{B} + \rho_e \vec{E}$$

where:

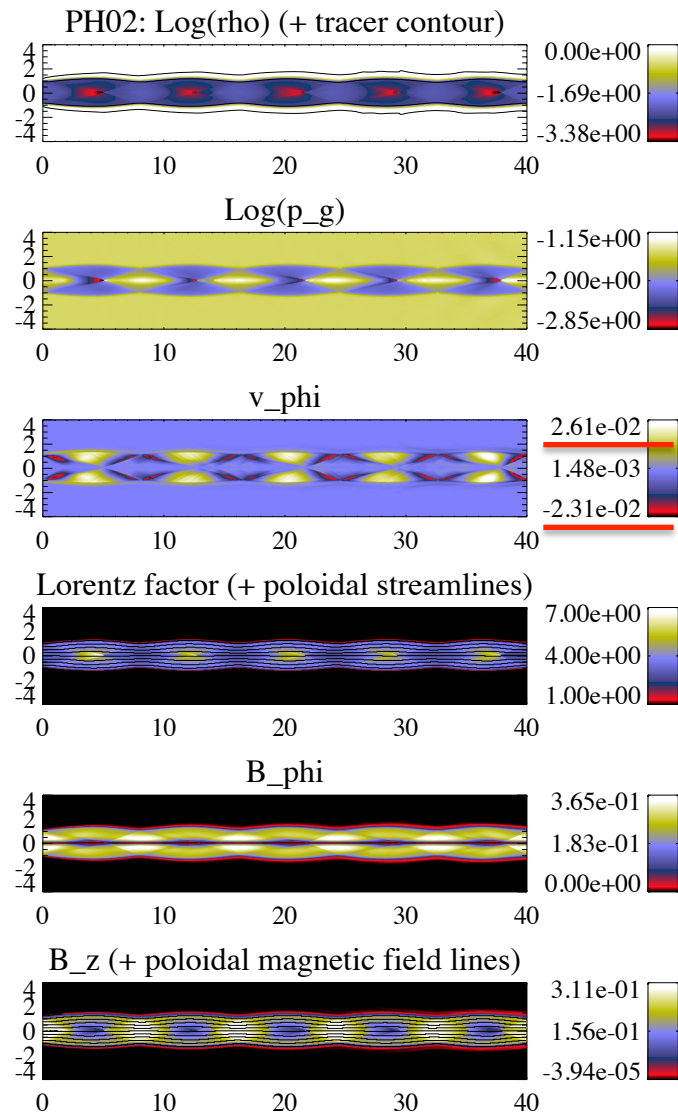
$$\vec{J} = \nabla \times \vec{B}, \quad \rho_e = \nabla \cdot \vec{E}, \quad \vec{E} = -\vec{v} \times \vec{B}$$

Azimuthal component:

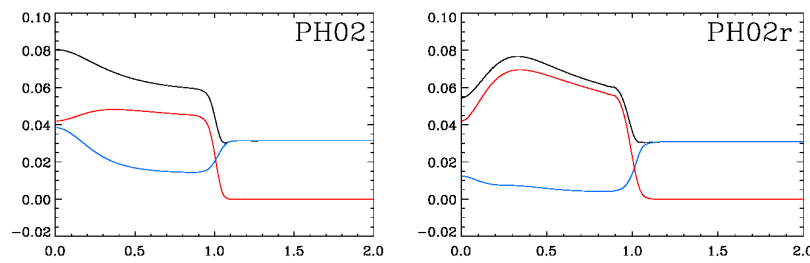
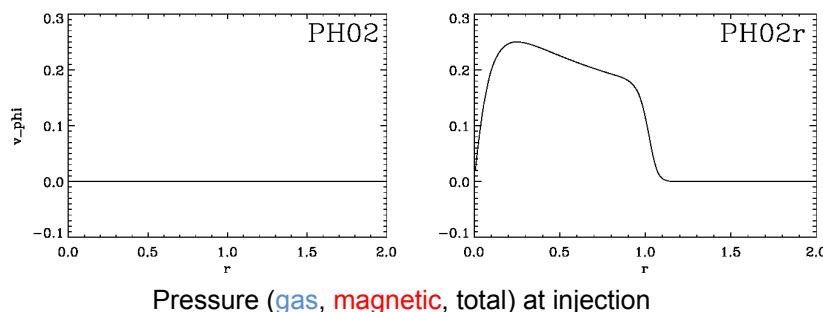
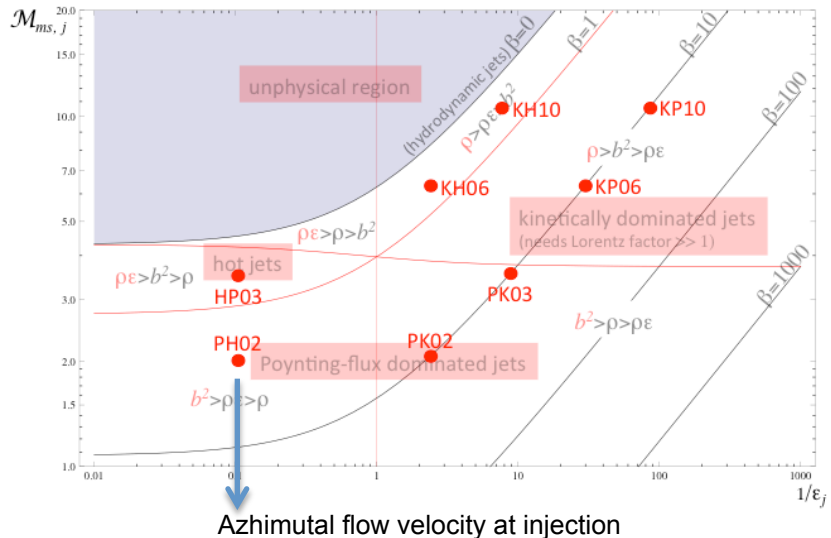
initially: 

$$F_L^\phi = B^z \frac{\partial B^\phi}{\partial z} + \frac{B^r}{r} \frac{\partial (r B^\phi)}{\partial r} + \rho_e (v^r B^z + v^z B^r)$$

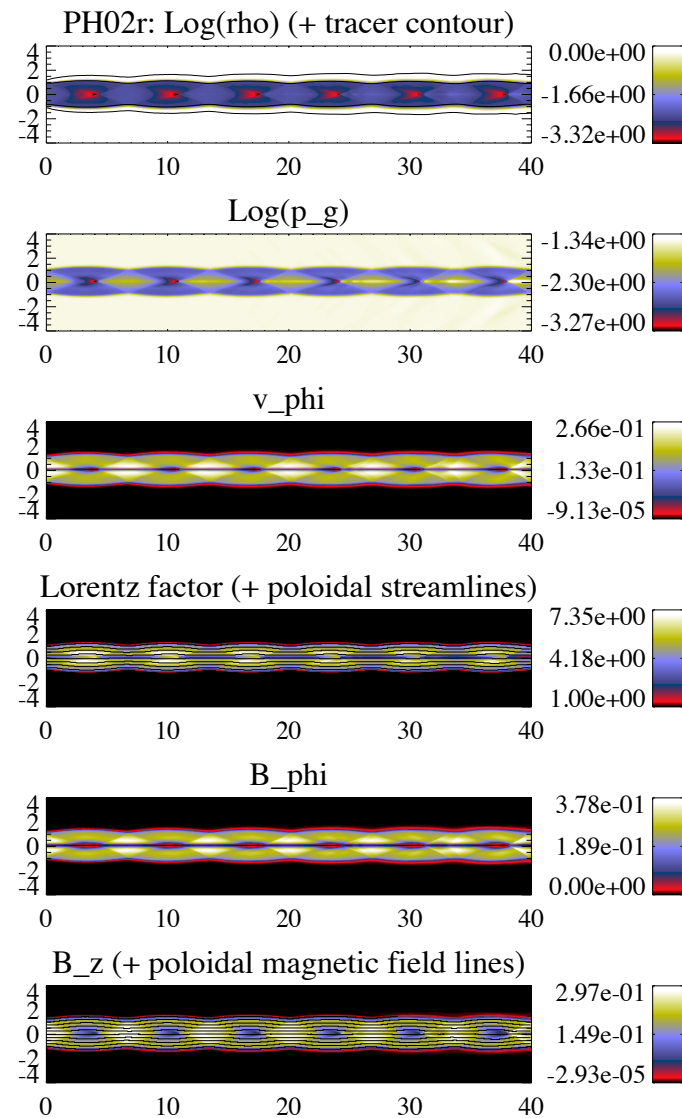
The speeds tend to be larger in models with maximum local opening angles (Hot jets)



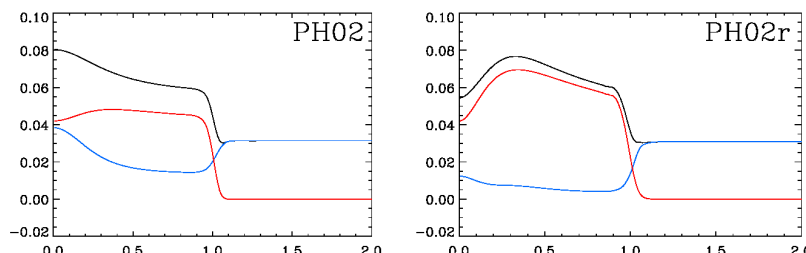
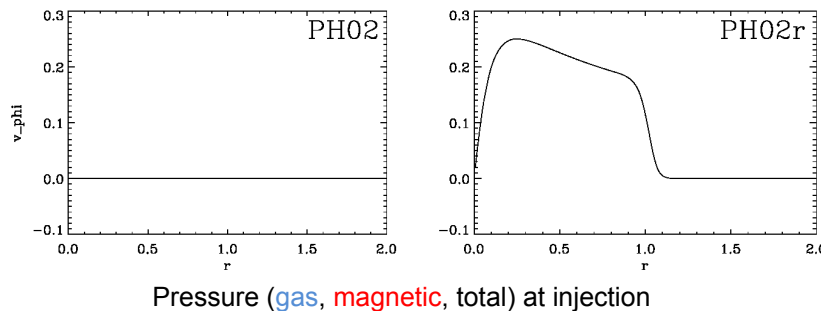
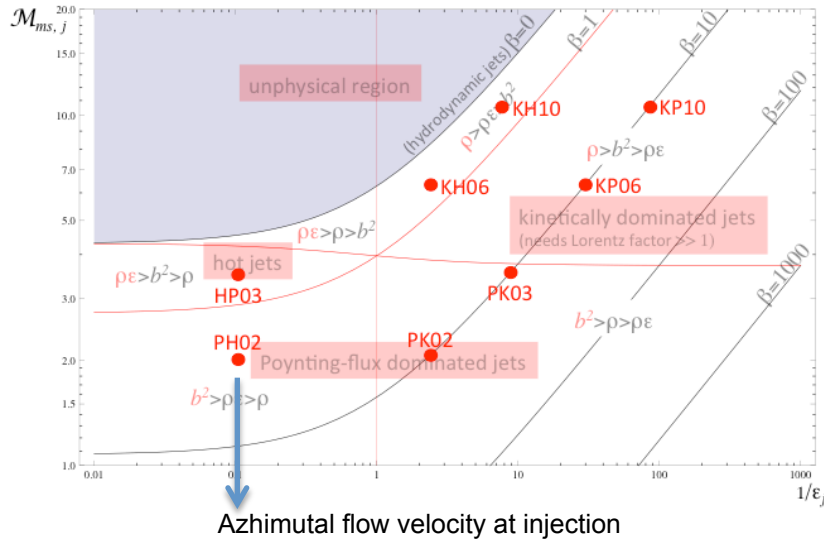
Internal structure of axisymmetric, overpressured RMHD jets: Effects of flow rotation (I)



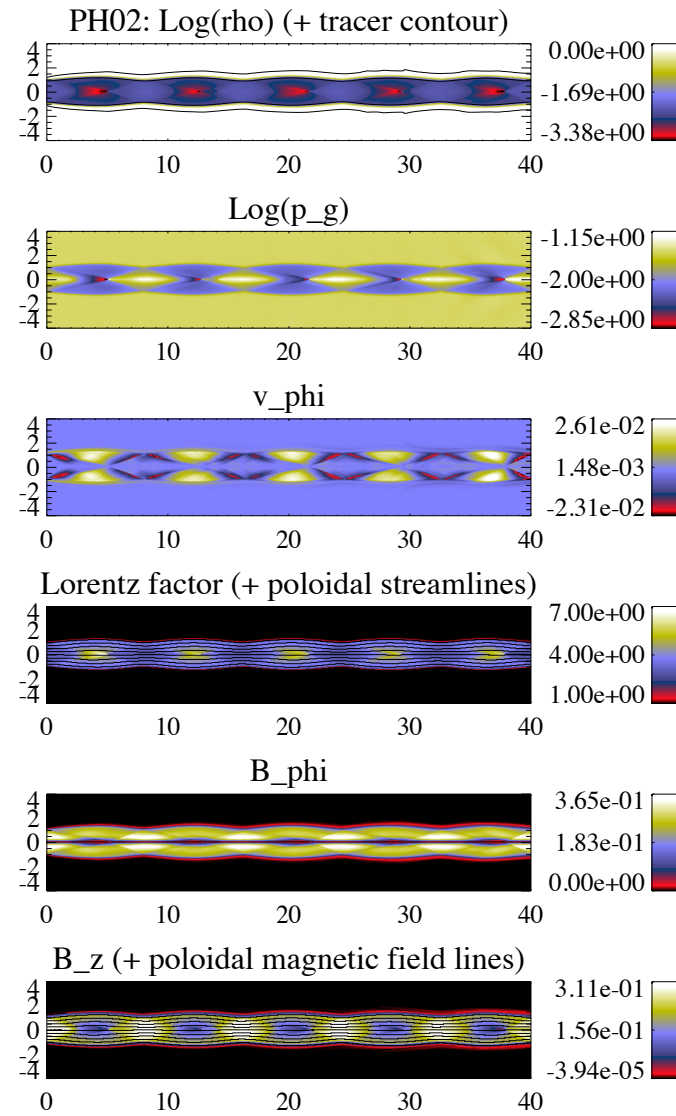
Rotation changes both gas and magnetic pressure



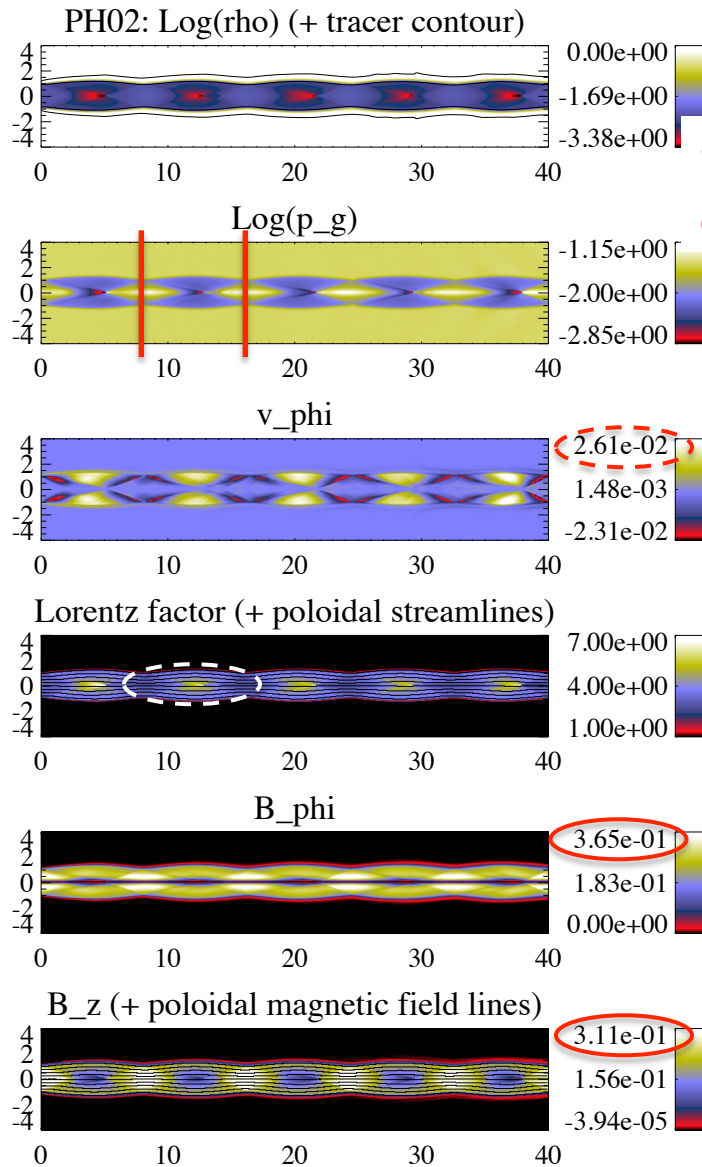
Internal structure of axisymmetric, overpressured RMHD jets: Effects of flow rotation (I)



Rotation changes both gas and magnetic pressure



Internal structure of axisymmetric, overpressured RMHD jets: Effects of flow rotation (II)

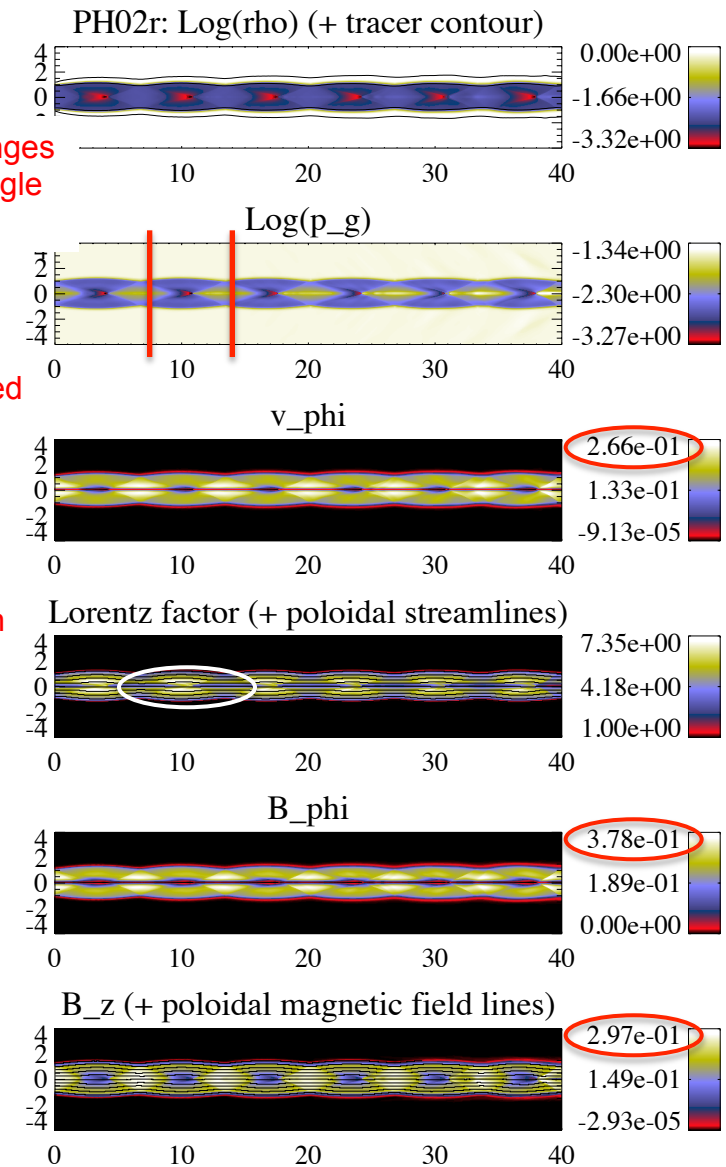


Shock periodicity changes by 20% (and shock angle changes accordingly)

v_phi reflects injected rotational profile

Lorentz factor fills the whole jet section

B_phi and B_z do not change much [as expected!]



Internal structure of axisymmetric, overpressured RMHD jets: Conclusions and future work

Models with a richer internal structure are those dominated by the internal energy (**hot jets, Poynting-flux dominated jets with low magnetization**)

- **strong quasi steady components** as a sign of high internal energy/low magnetization

“Hot” spines around the axis are found in **high-magnetization jets**, due to the magnetic tension of the toroidal field

- observational counterpart?

Poynting flux dominated jets are prone to be **unstable against magnetic pinch modes**

- “Real” jets have **small magnetizations** (~ 1) or need to be stabilized by a **wide shear layer** (must leave observational imprints)

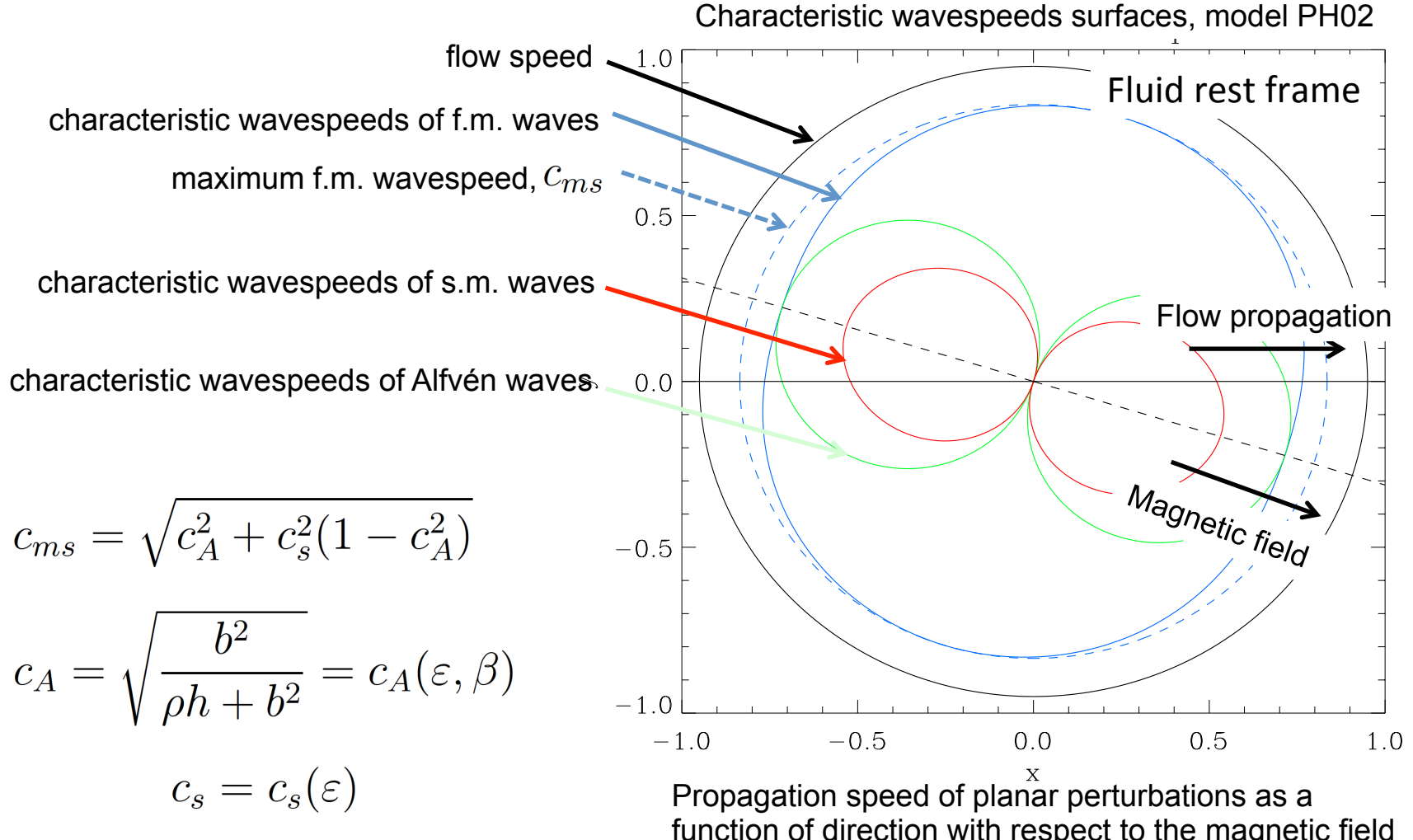
Small (non-zero) azimuthal flow velocities are generated in all the models in regions of jet expansion/contraction under the action of the Lorentz force

- **asymmetries in total and polarized emission**

Future work:

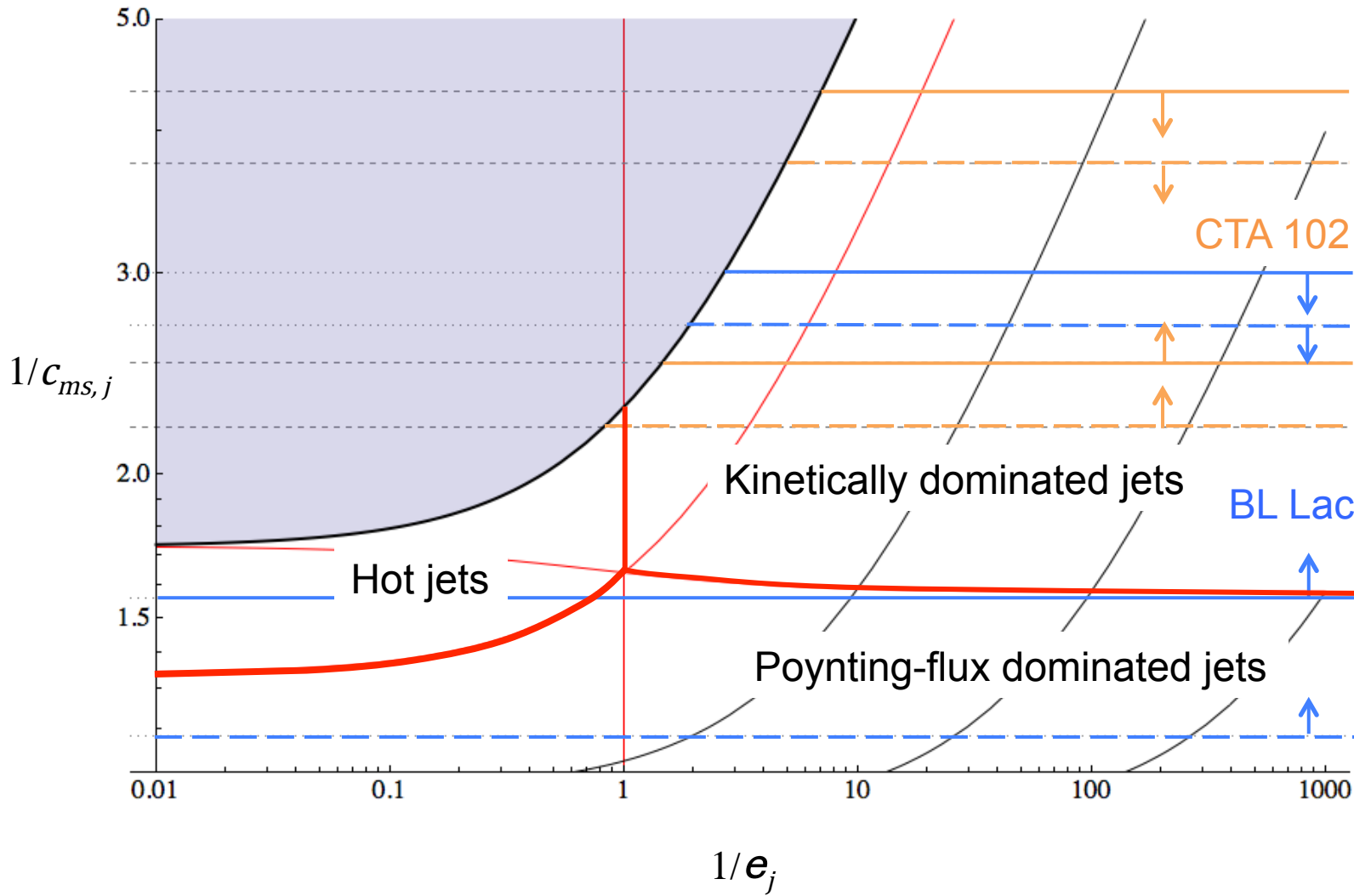
- extend the present study to other parameters (**jet rotation, overpressure factor, magnetic pitch angle**) [First models with large flow rotation speeds analyzed]
- compute the **synchrotron emission** of the models and look for observational counterparts
- Include **traveling shocks** and **external pressure gradients**

Magnetosonic Mach number versus specific internal energy diagram

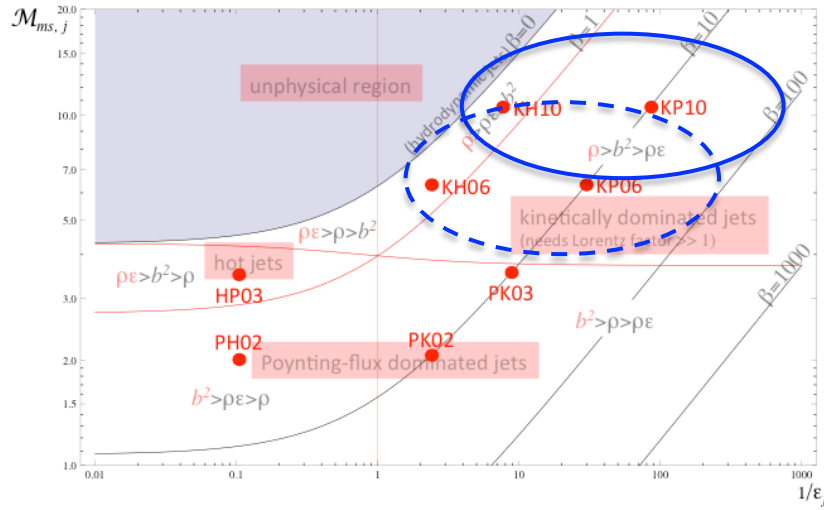


$$\mathcal{M}_{ms} = \frac{W}{W_{ms}} \frac{v}{c_{ms}} = \mathcal{M}_{ms}(W, \varepsilon, \beta)$$

(classical) Magnetosonic Mach number versus specific internal energy
 (for large Lorentz factor jets)

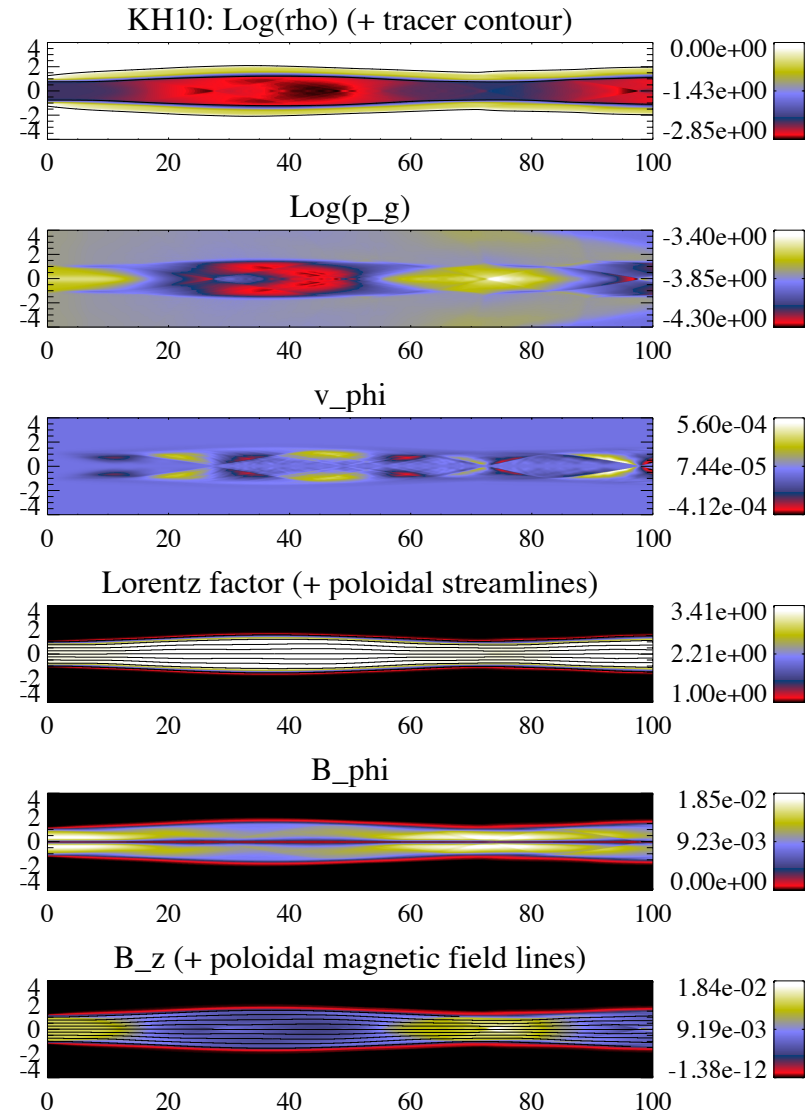


Internal structure of axisymmetric, overpressured RMHD jets: Results (II)



Kinetically dominated jets (KH10, KP10):

- Poor internal structure characterized by radial jet oscillations with long-wavelength axial periodicity
- No internal energy to exchange for kinetic energy
[Bernoulli mechanism does not operate]
- Almost constant flow Lorentz factor
- “Hot” central spine in high-magnetization jets, due to the magnetic tension of the toroidal field



RMHD code (I): code characteristics and order of convergence in 1D smooth tests

Solves the equations of **(ideal) relativistic magneto-hydrodynamics equations** in conservation form for an **ideal gas equation of state**

2.5D planar-symmetric (Cartesian coordinates) and axially-symmetric (cylindrical/spherical coordinates)

Second-order, conservative, finite-volume, constrained-transport code based on high-resolution shock-capturing techniques:

- **Cell reconstruction:** reconstruction of primitive variables with **piecewise linear functions and slope limiters (MINMOD, VANLEER, MC)**
- **Riemann solvers:** **HLL, HLLC**
- **Time advance:** second and third order **TVD-RK methods**
- **Constrained Transport scheme:** **Balsara and Spicer (1999) + correction of conserved variables** in high magnetization flows
- **Primitive variable recovery by bisection**

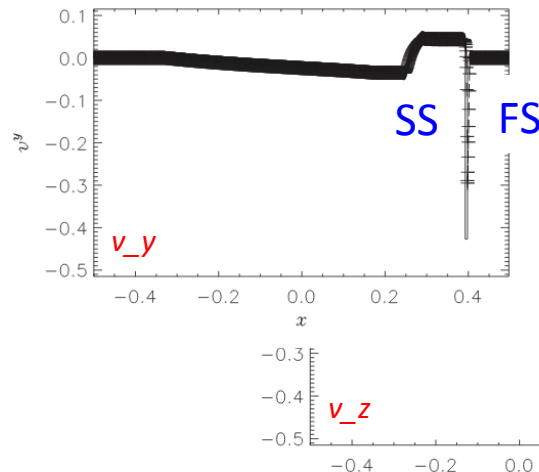
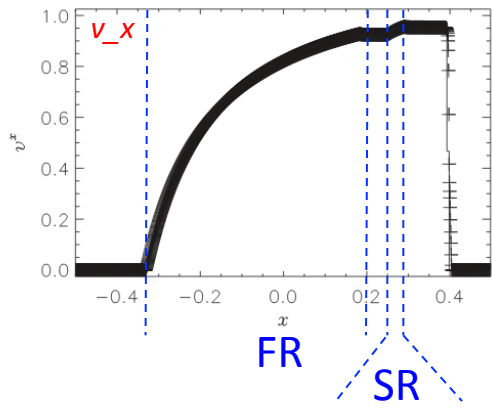
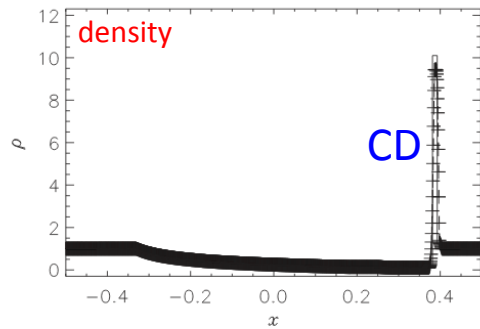
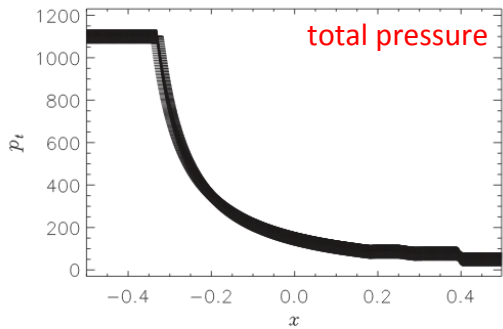
Code and tests details: [Martí 2015a, 2015b](#)

State-of-art of numerical RMHD: [Martí and Müller 2015](#)

Table B1. Accuracy of the code from the circularly polarized Alfvén wave test.

Method	N	L_1 error	L_1 order
MINMOD	8	1.83×10^{-1}	–
	16	8.16×10^{-2}	1.17
	32	2.19×10^{-2}	1.90
	64	5.47×10^{-3}	2.00
	128	1.51×10^{-3}	1.86
	256	4.05×10^{-4}	1.90
	512	1.05×10^{-4}	1.95
	VAN LEER	1.49×10^{-1}	–
VAN LEER	8	3.96×10^{-2}	1.91
	16	7.86×10^{-3}	2.33
	32	1.58×10^{-3}	2.31
	64	3.55×10^{-4}	2.15
	128	8.36×10^{-5}	2.09
	256	2.01×10^{-5}	2.07
	512	1.26×10^{-1}	–
	MC	2.70×10^{-2}	2.22
MC	8	5.45×10^{-3}	2.31
	16	1.28×10^{-3}	2.09
	32	3.13×10^{-4}	2.03
	64	7.75×10^{-5}	2.01
	128	1.93×10^{-5}	2.01

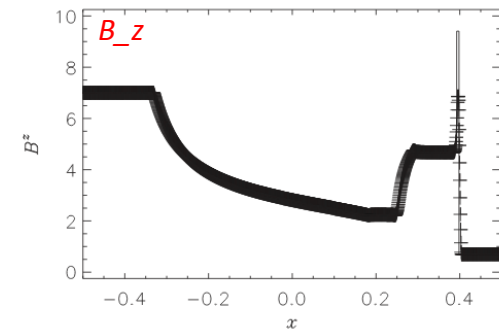
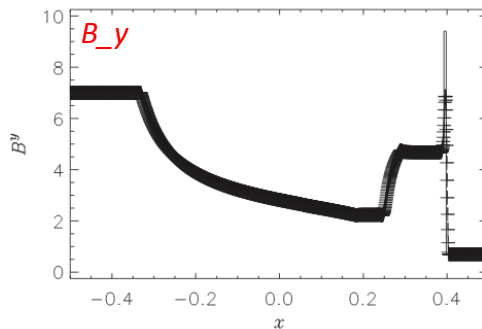
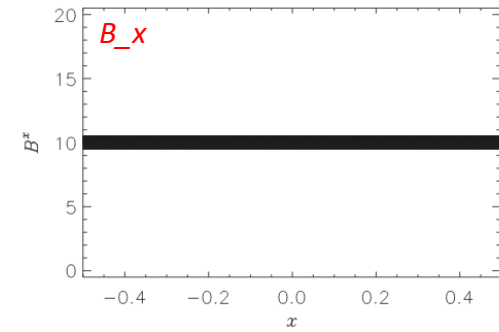
RMHD code (II): 1D tests with discontinuities and thin structures



Riemann problem #3 in Balsara (2001)

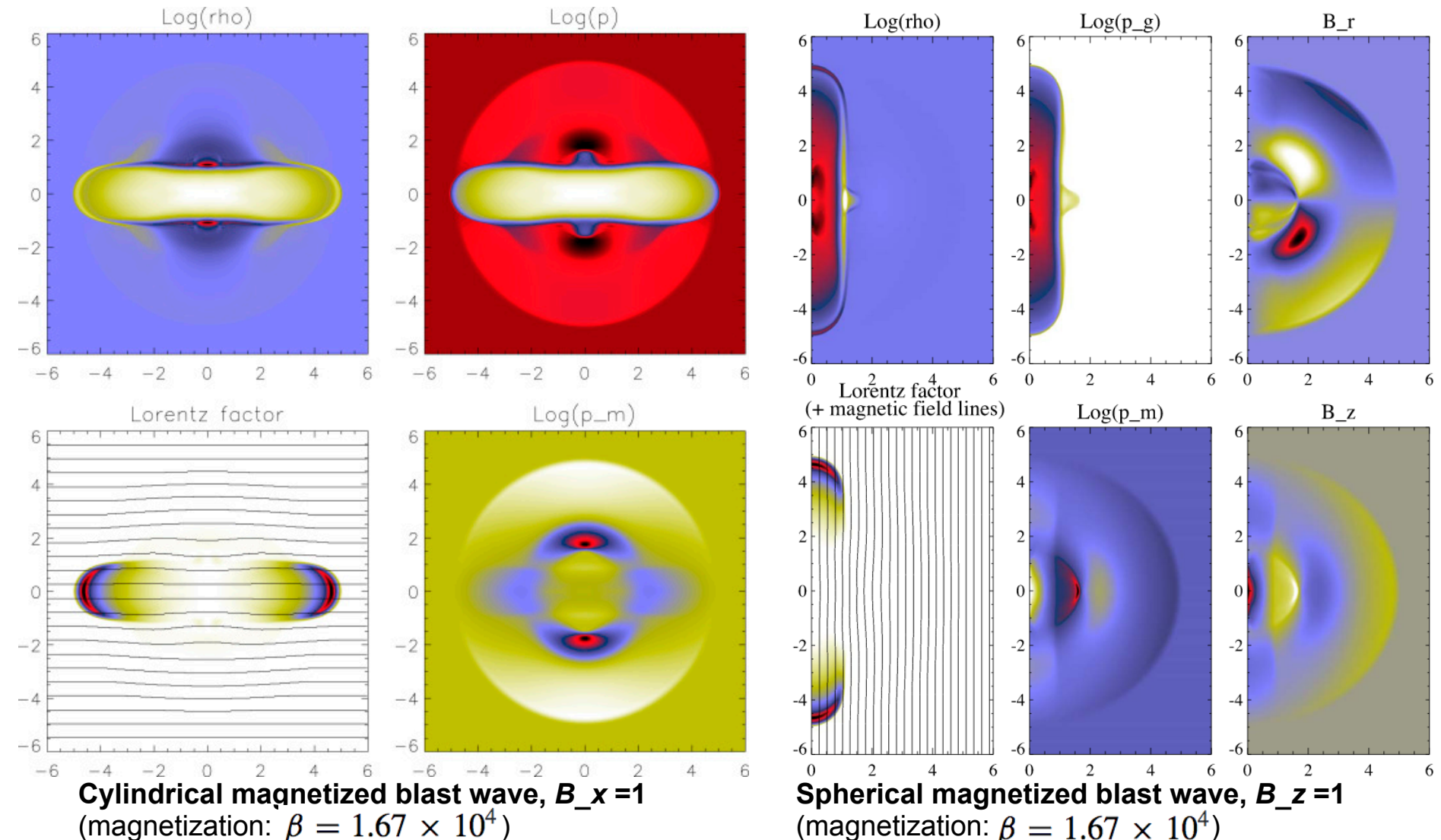
1600 cells, MC limiter, HLLC Riemann solver, 3rd order TVD-RK for time advance

Analytical solution (Giacomazzo & Rezzolla 2006) overimposed



The solution is composed of two left-going fast and slow rarefactions (FR, SR), a contact discontinuity (CD) and two right-going fast and slow shocks (FS, SS)

RMHD code (III): Multidimensional test problems



Cylindrical magnetized blast wave, $B_x = 1$
 (magnetization: $\beta = 1.67 \times 10^4$)

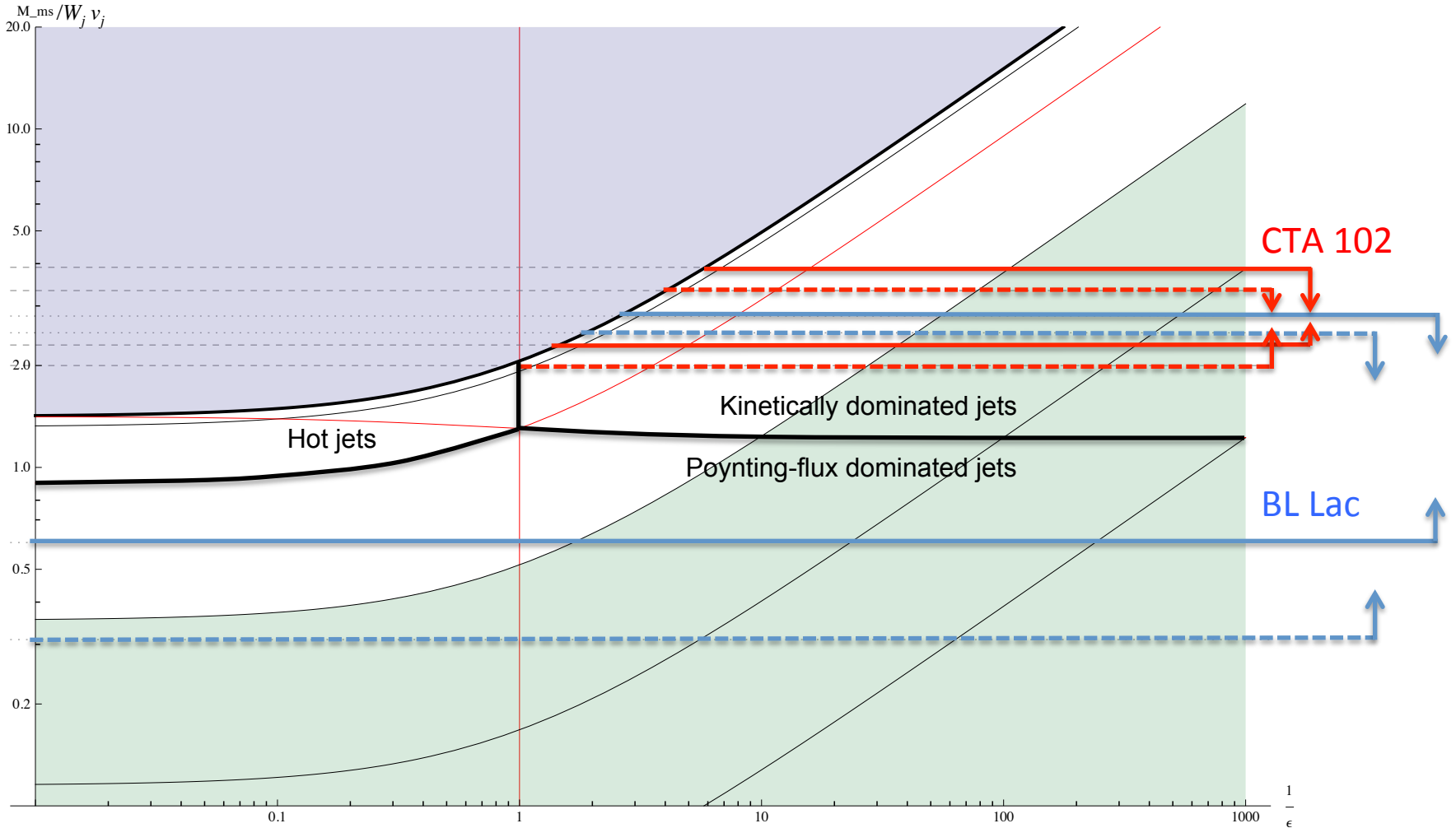
Cartesian coordinates

512² cells, VLMM limiter, HLLC Riemann solver, 3rd order TVD-RK for time advance

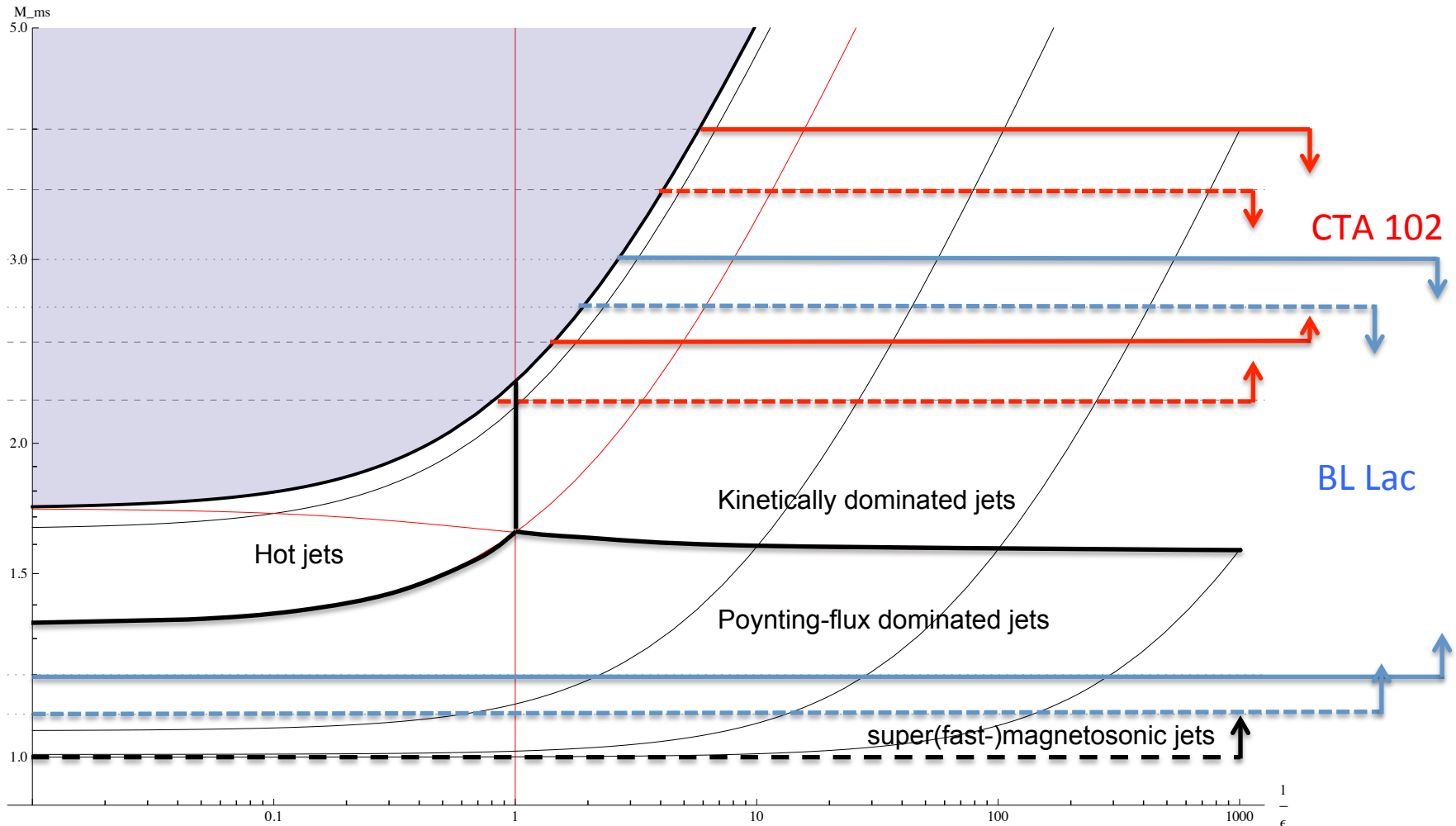
Spherical magnetized blast wave, $B_z = 1$
 (magnetization: $\beta = 1.67 \times 10^4$)

Cylindrical coordinates

512 x 1024 cells, VLMM limiter, HLL Riemann solver, 3rd order TVD-RK for time advance



(classical) Magnetosonic Mach number versus specific internal energy
 (for jets with large flow Lorentz factors)



(classical) Magnetosonic Mach number versus specific internal energy
(for large Lorentz factor jets)

